DALTON
FULL PAPER

On the rational synthesis and properties of exchange-coupled heterotrinuclear systems containing $[M_AM_BM_B]$ and $[M_AM_BM_C]$ cores †

Cláudio Nazari Verani, Eva Rentschler, Thomas Weyhermüller, Eckhard Bill and Phalguni Chaudhuri *

Max-Planck-Institut für Strahlenchemie, Stiftstraße 34-36, D-45470 Mülheim an der Ruhr, Germany. E-mail: chaudh@mpi-muelheim.mpg.de

Received 18th July 2000, Accepted 2nd October 2000
First published as an Advance Article on the web 14th November 2000

Six new modular linear heterotrinuclear complexes of the types $[M_AM_BM_B]$ and $[M_AM_BM_C]$ with $Fe^{III}Cu^{II}Ni^{II}$ **1**, $Fe^{III}Ni^{II}Ni^{II}$ **2**, $Co^{III}Cu^{II}Ni^{II}$ **3**, $Fe^{III}Cu^{II}Cu^{II}$ **4**, $Fe^{III}Ni^{II}Cu^{II}$ **5** and $Fe^{III}Mn^{II}Cu^{II}$ **6** cores were synthesized using selective template reactions involving the ligands 1,4,7-trimethyl-1,4,7-triazacyclononane, tmtacn, and *N*,*N*′-bis(2-hydroxy-3-hydroxyiminomethyl-5-methylphenylmethylene)-1,3-propanediamine, H_4Lox. The complexes were characterised by elemental analysis (C, H, N, and the metals), IR, UV-vis, Mössbauer and EPR spectroscopies and variable temperature and variable field magnetic susceptibility measurements. The crystal structure of **2** was determined by X-ray diffraction. It is comparable to those of the previously published compounds **1** and **3** and consists of high-spin Fe^{III} and six-co-ordinated Ni^{II} embedded in the imine–oxime ligand, with an intramolecular Fe · · · Ni distance of 3.79 Å and Ni · · · Ni distance of 3.14 Å. The magnetic behaviour of the compounds is complex and exhibits a predominant antiferromagnetic exchange coupling acting along the pathway $d_{x^2-y^2}\|sp^2\|d_{x^2-y^2}\|sp^2\|d_{x^2-y^2}$. The coupling constant $J_{MA\text{-}MB}$ ranges from −5 to −20 cm^{-1}, while $J_{MB\text{-}MC}$ ranges from −66 to −395 cm^{-1} (except for $J_{Ni\text{-}Ni} = -21$ cm^{-1}). The coupling constant $J_{MA\text{-}MC}$ was kept fixed to zero during the fitting procedure. Compounds **1** and **5** with isoelectronic structures exhibit ground and first excited states inverted to one another due to their spin topology.

Introduction

Exchange coupled polymetallic complexes, in which spin coupling between paramagnetic metals is propagated *via* bridging atoms, are of special interest to researchers seeking new molecule-based magnetic materials displaying interesting electronic properties and to bioinorganic chemists investigating the structure and function of polynuclear metal centres in proteins. Thus, during the last two decades polynuclear systems have drawn attention particularly of inorganic chemists, as they constitute a common ground for symbiosis of two apparently different subjects, *viz*. molecular magnetism[1] and bioinspired and/or biomimicking chemistry.[2] Of particular concern in this context is the development of synthetic routes that can provide mixed-metal complexes with high nuclearity in a controlled fashion. Amongst the variety of methodologies applied to synthesize polymetallic co-ordination compounds, the use of "metalloligands", *i.e*. metal complexes as ligands,[3] has proven to be very successful; this route involving multinucleating ligands offers many potential advantages over the self-assembly route in that it enables more stringent control over the course of the reaction and upon the products that form. We have favoured the strategy of "metal oximate" building blocks as ligands to design and synthesize high nuclearity complexes in a controlled fashion.[4] This approach of using metalloligands containing polynucleating ligands proceeds step by step and provides a route to gain control of the nuclearity in addition to the preparation of species containing different metal ions, *i.e*. heterometallic complexes.

In recent papers[5,6] we have reported several modular complexes containing the end-capping amine 1,4,7-trimethyl-1,4,7-triazacyclononane (tmtacn) and several bridging oximes. These studies were aimed at providing some answers to questions regarding the exchange mechanisms in compounds comprising $[M_AM_B]$ (a, b), $[M_AM_BM_A]$ (c), $[M_AM_BM_BM_A]$ (d), $[(M_A)_2(\mu\text{-}O)_2(M_B)_2]$ (e) cores which are represented in Scheme 1.

Herein we report the rational synthesis, spectroscopic and magnetic properties of a series of complexes $[(tmtacn)M_A(Lox)M_BM_C]^{3+}$, where $M_A = Fe^{III}$ or Co^{III} is facially co-ordinated to the amine tmtacn and $M_B = Cu^{II}$, Ni^{II} or Mn^{II} and $M_C = Cu^{II}$ or Ni^{II} are embedded in the asymmetric dicompartmented imine–oxime ligand H_4Lox, shown below.

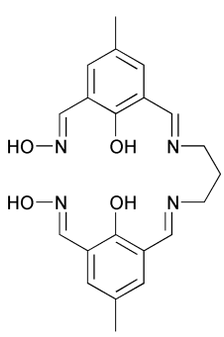

The structure of the compound with $M_A = Fe^{III}$, $M_B = M_C = Ni^{II}$, $Fe^{III}Ni^{II}Ni^{II}$, as well as its comparison with other similar compounds, *viz*. $Fe^{III}Cu^{II}Ni^{II}$ and $Co^{III}Cu^{II}Ni^{II}$ whose structures are already published,[6] are also included. The general framework for the heterotrinuclear complexes is depicted below.

† Electronic supplementary information (ESI) available: IR spectra of the heteronuclear complexes. See http://www.rsc.org/suppdata/dt/b0/b005768l/

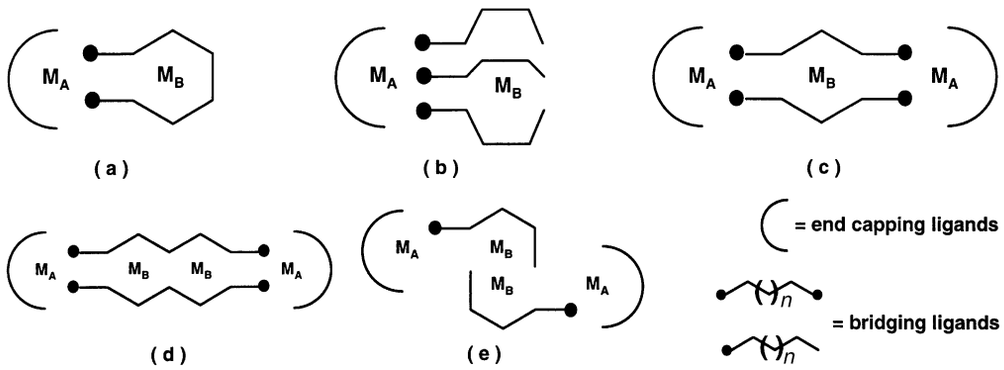

Scheme 1 General representation of modular heteropolynuclear complexes.

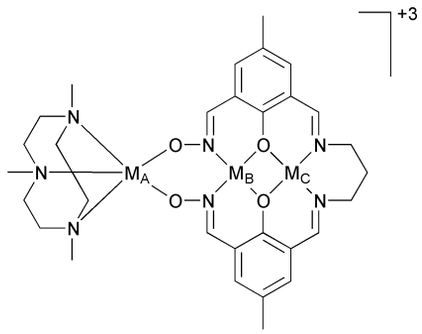

It is worth mentioning in this connection that the presence of different competing interactions owing to the topologies in polynuclear complexes may lead to ground and other low-lying states that cannot be expected by simple combination of the local spins according to the nature of the interactions present between the spin carriers. We will demonstrate in this paper one such example of "ground-state variability".

For the sake of clarity the aforementioned complexes are denoted only by the metal centres throughout this paper.

Results and discussion

Preparation and characterisation of the complexes

Synthesis. The synthesis of the heterotrinuclear complexes involves several sequential steps. Binuclear imine–oxime complexes with the core $[M_C^{II}M_B^{II}(L)]$ can be synthesized by the addition of the metal M_B as its chloride salt to the mononuclear species $[M_C(L)]$ (where $M_C = Cu^{II}$ or Ni^{II} and L is the Schiff base condensation product of 2,6-diformyl-4-methylphenol (2 equiv.) and 1,3-diaminopropane (1 equiv.)) in MeOH. Complex $[M_C^{II}M_B^{II}(L)]Cl_2$ in a subsequent step is treated with NH_2OH to yield the target molecule $[M_C^{II}M_B^{II}(HLox)]^+$. This method is very effective, albeit somewhat more time consuming. Addition of the second metal ion M_B and NH_2OH for a template-assisted oxime formation[7] is also possible. Although the oxime synthons $[M_C^{II}M_B^{II}(HLox)]^+$ with cores $[Cu^{II}Pb^{II}]$, $[Cu^{II}Zn^{II}]$, $[Cu^{II}Cu^{II}]$, $[Cu^{II}Ni^{II}]$, $[Cu^{II}Co^{II}]$, $[Cu^{II}Mn^{II}]$, $[Cu^{II}Mg^{II}]$, $[Ni^{II}Cu^{II}]$ and $[Ni^{II}Ni^{II}]$ were isolated, it was not possible, however, to convert all of these species into the trinuclear complexes, presumably because of metal scrambling processes. Hence we are refraining from describing the above mentioned binuclear oximes $[M_BM_C(HLox)]^+$ in this paper. The dinuclear precursor $[Ni^{II}Ni^{II}]$ has been reported by other groups.[8] The last step in the synthesis of the target molecules involves the reaction of the binuclear synthons with the Fe^{III}(tmtacn) or the Co^{III}(tmtacn) unit, prepared *in situ* by reaction of end-capping tmtacn in MeOH with $CoCl_2$ in the presence of Et_3N and air. The purpose of the added base is to provide a basic medium needed for deprotonation of the hydrogen bridged oxygen atoms, OH···O, present in most solid oximes and to oxidise the cobalt centre by air. The reaction leads to formation of the $[M_A^{III}M_B^{II}M_C^{II}]$ heterotrinuclear compounds. Trinuclear complexes synthesized and characterised are: **$Fe^{III}Cu^{II}Ni^{II}$ 1**, **$Fe^{III}Ni^{II}Ni^{II}$ 2**, **$Co^{III}Cu^{II}Ni^{II}$ 3**, **$Fe^{III}Cu^{II}Cu^{II}$ 4**, **$Fe^{III}Ni^{II}Cu^{II}$ 5**, **$Fe^{III}Mn^{II}Cu^{II}$ 6**.

IR spectra. Although IR spectra could not identify the individual metals and their ratios in the polynuclear complexes, the $\nu_{C=O}$ and $\nu_{C=N}$ stretching region 1700–1500 cm^{-1} appeared to be most diagnostic during the various synthetic stages, as is exemplified in the Supplementary Material.

The complexes [Ni(L)] and [Cu(L)] exhibit peaks at *ca.* 1665–1670 cm^{-1}, attributable to the carbonyl stretching ($\nu_{C=O}$) of the aldehyde. The imine C=N stretch ($\nu_{C=N}$) appears at 1625–1630 cm^{-1}. Another peak at around 1545 cm^{-1} is attributed to skeletal vibrations.[9] The peak at 1665–1670 cm^{-1} disappears during formation of the binuclear species $[M_CM_B(L)]^{2+}$. On the other hand, further addition of the second metal in the presence of NH_2OH leads to a template-assisted formation of $[M_CM_B(HLox)]^+$ and peaks due to N–O appear at *ca.* 1230 and 1180 cm^{-1}, as expected for oxime complexes.[10] The peak around 1310 cm^{-1} is attributed to the phenolate group ν_{C-O}. The oxime C=N stretch ($\nu_{C=N}$) seems to be overlapped by that of the $C=N_{imine}$ fragment. This notion is reinforced by the observation of a single strong peak at *ca.* 1630 cm^{-1}. The heterotrinuclear complexes exhibit new peaks at 2930, 1495, 1465, 810, and 760 cm^{-1} which are attributed to the end-capping amine tmtacn. In the compounds described here the trivalent metal ion is co-ordinated to the binuclear oxime synthon through the oxygen atoms. This co-ordination stabilises the negative charge on the oxygen atoms and consequently contributes to stabilisation of the C=N character and further partial π delocalisation in the aromatic ring. It is generally accepted that the higher the positive charge on the terminal ion, the stronger is the C=N bond and weaker the N=O character.[10] Non-co-ordinated perchlorate counter ions show a strong band at *ca.* 1085 cm^{-1} (antisymmetric stretch) and a comparatively weak but sharp band at *ca.* 623 cm^{-1} (antisymmetric bend). The low energy ν_{N-O} peak expected at around 1100–1085 cm^{-1} is overlapped by these peaks. Compound **$Fe^{III}Ni^{II}Ni^{II}$ 2** contains co-ordinated SCN groups as is evident from the strong peaks at 2100 and 1055 cm^{-1}.

UV-vis spectra. All the compounds exhibit similar spectral features in the UV-vis region with four bands at *ca.* 280 ($\varepsilon > 7500$), 370 (≈ 3500), 450 nm (≈ 1100) and 550 nm (≈ 500 M^{-1} cm^{-1}). No bands are observed in the range 700–1100 nm. The first band below 300 nm is assigned to a ligand transition ($\pi \longrightarrow \pi^*$). The bands at *ca.* 370 and 450 nm are attributed to CT processes, the former being assigned to $e_g \longrightarrow \pi^*_{oxime}$ metal-to-ligand transitions. Such transitions are characteristic for complexes where oxidisable metals are bonded to unsaturated ligands with empty antibonding π orbitals. The lower energy band is present as a shoulder and tentatively attributed to ligand-to-metal CT from the phenolate groups to the M_B and

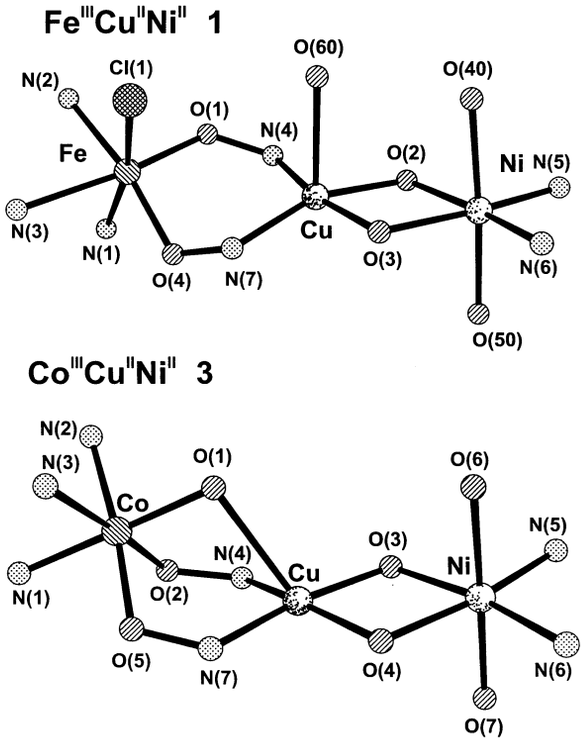

Fig. 1 Perspective views of complexes **1** and **3** highlighting the donor atoms of the respective metal centres in the cores.

M_C centres. This band is overlapped in complexes **4** and **6**. Although both CT transitions are relatively weak, such assignments and absorption coefficients of similar environments are well documented.[11] The weaker transitions at *ca*. 550 nm appear in the expected ligand-field region and are assumed to be d–d transitions. The comparatively high absorption coefficients can be explained by extensive mixing of the metal and the ligand orbitals arising from the low symmetry at the metal centres.[5b] Finally the electronic spectral data support the idea that the complexes are stable and retain their discrete trinuclear entity also in solution.

Structure descriptions

The complexes $Fe^{III}Cu^{II}Ni^{II}$ 1 and $Co^{III}Cu^{II}Ni^{II}$ 3. The molecular structures of complexes **1** and **3** were reported in previous papers.[6] Salient features are summarised here for comparison purposes. The core of both complexes is depicted in Fig. 1.

Both complexes consist of discrete heterotrinuclear units. Compound **1** exhibits intramolecular distances Fe···Cu 3.695(1), Cu···Ni 3.087(1) and Fe···Ni 6.772(1) Å, whereas in **3** the distances are Co···Cu 3.299(1), Cu···Ni 3.081(1) and Co···Ni 6.236(1) Å. These distances are in agreement with those in similar compounds described by us[3f,5e] and others.[3d,12,13] Interestingly, **1** presents an almost linear metal framework with the Fe–Cu–Ni angle being 174.0(1)°. By contrast, the central Cu^{II} in **3** adopts a distorted square pyramidal geometry arising from the presence of a μ-OH bridge to cobalt (angle Co–O–Cu 98.1(2)°), thus resulting in a loss of linearity with an angle Co–Cu–Ni of 155.6(2)°.

Complex $Fe^{III}Ni^{II}Ni^{II}$ 2. The structure of this compound consists of a discrete neutral trinuclear unit [(tmtacn)Fe^{III}(NCS)-Ni^{II}(H_2O)(NCS)Ni^{II}(NCS)(H_2O)(Lox)]·2MeCN. One SCN group is co-ordinated to each of the three metal centres in N-bonded fashion. An ORTEP[14] plot with the atom labelling scheme is presented in Fig. 2. Table 1 summarises selected bond lengths and angles.

The iron centre Fe(1) is co-ordinated facially to N(1) (2.204(5)), N(2) (2.235(5)), and N(3) (2.241(4) Å) from the ligand tmtacn and to two oxygen atoms O(1) and O(4) (av. 1.89(1) Å) from the oxime groups of Lox and to N(40) (2.064(5) Å) from SCN forming a pseudo-octahedral environment. The N–O bond lengths (≈ 1.38 Å) and C–N–O angles (111.9(6)°) indicate sp^2 hybridisation. Both the nickel ions are in distorted octahedral N_3O_3 environments. The first, Ni(1), is co-ordinated to two nitrogen atoms, N(4) at 2.006(5) and N(7) at 2.022(4) Å, from the oxime groups and to the oxygen atoms O(2) and O(3), 2.053(3) and 2.026(4) Å, respectively, from the phenolate groups of the ligand Lox^{4-}. The co-ordination sphere is completed by a water molecule, Ni(1)–O(50) at 2.232(5) Å, and an N-co-ordinated SCN group, Ni(1)–N(50) at 2.062(6) Å, which are bonded axially. The second nickel centre Ni(2) exhibits a similar environment with comparable bond lengths, although the nitrogen atoms N(5) and N(6) belong to the imine portion of the ligand with C=N bonds at av. 1.282(6) Å. The axial SCN group Ni(2)–NCS is at 2.113(6) Å. It is noteworthy that each of the similar axial ligands, NCS and H_2O, at both nickel centres are *trans* to one another. The distances between the metal centres are 3.793(1) Å for Fe···Ni(1) and 3.144(1) Å for Ni(1)···Ni(2) whereas the bridging angles Ni(1)–O(2)–Ni(2) and Ni(1)–O(3)–Ni(2) are 100.5(2) and 102.1(2)°, respectively.

The angle Fe–Ni(1)–Ni(2) is 170.5(4)°. The bond length and angles are in accord with complex **1** and with those in other

Table 1 Selected distances (Å) and angles (°) for $Fe^{III}Ni^{II}Ni^{II}$ **2**

Fe–N(1)	2.204(5)	Ni(2)–O(60)	2.219(5)
Fe–N(2)	2.235(5)	Ni(2)–N(5)	2.014(4)
Fe–N(3)	2.241(4)	Ni(2)–N(6)	2.023(5)
Fe–N(40)	2.064(5)	Ni(2)–N(60)	2.113(6)
Fe–O(1)	1.894(3)		
Fe–O(4)	1.878(4)	O(1)–N(4)	1.379(5)
		O(4)–N(7)	1.383(5)
Ni(1)–N(4)	2.006(5)	C(12)–O(2)	1.313(6)
Ni(1)–N(7)	2.022(4)	C(24)–O(3)	1.329(6)
Ni(1)–N(50)	2.062(6)	C(18)–N(5)	1.274(6)
Ni(1)–O(2)	2.053(3)	C(22)–N(6)	1.284(6)
Ni(1)–O(3)	2.026(4)		
Ni(1)–O(50)	2.232(5)		
		Fe···Ni(1)	3.793(1)
Ni(2)–O(2)	2.037(4)	Ni(1)···Ni(2)	3.144(1)
Ni(2)–O(3)	2.017(3)	Fe···Ni(2)	6.937(1)
N(1)–Fe–N(40)	168.0(2)	N(50)–Ni(1)–O(50)	173.2(2)
N(2)–Fe–O(4)	167.5(2)	N(4)–Ni(1)–N(7)	100.9(2)
O(1)–Fe–O(4)	100.5(2)	O(3)–Ni(2)–N(5)	169.5(2)
O(1)–Fe–N(3)	165.8(2)	O(60)–Ni(2)–N(60)	170.2(2)
O(2)–Ni(1)–O(3)	78.42(14)	O(2)–Ni(1)–O(3)	79.00(13)
C(30)–N(7)–O(4)	111.3(4)	N(5)–Ni(2)–N(6)	98.8(2)
C(10)–N(4)–O(1)	112.6(4)	Fe(1)–O(4)–N(7)	132.0(3)
N(4)–Ni(1)–O(2)	168.1(2)	Fe(1)–O(1)–N(4)	125.4(3)
N(7)–Ni(1)–O(3)	162.8(2)	Fe–Ni(1)–Ni(2)	170.5(4)

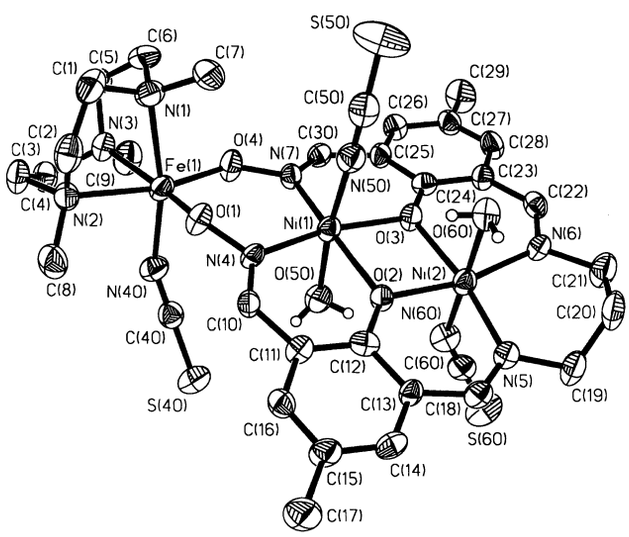

Fig. 2 An ORTEP plot and labelling scheme for $Fe^{III}Ni^{II}Ni^{II}$ **2**.

Table 2 Magnetic properties of the heterotrinuclear complexes

Compound $[M_AM_BM_C]$	J_{AB}/ cm^{-1}	J_{BC}/ cm^{-1}	g_A	g_B	g_C	δ/ mm s^{-1}	ΔE_Q/ mm s^{-1}	Reference
1 $Fe^{III}Cu^{II}Ni^{II}$	−19.8	−118.6	2.0	2.10	2.20	0.46	0.85	This work, 6(*a*)
2 $Fe^{III}Ni^{II}Ni^{II}$	−9.3	−21.4	2.0	2.28	2.28	0.47	0.59	This work
3 $Co^{III}Cu^{II}Ni^{II}$	—	−130.2	—	2.24	2.27	—	—	This work, 6(*b*)
4 $Fe^{III}Cu^{II}Cu^{II}$	−5.0	−395.0	1.98	2.10	2.10	0.47	0.78	This work
5 $Fe^{III}Ni^{II}Cu^{II}$	−10.6	−161.5	2.0	2.30	2.10	0.47	0.77	This work
6 $Fe^{III}Mn^{II}Cu^{II}$	−12.6	−66.8	2.0	2.00	2.10	0.44	0.27	This work

J_{AC} values were fixed at 0.0 cm^{-1} in all cases.

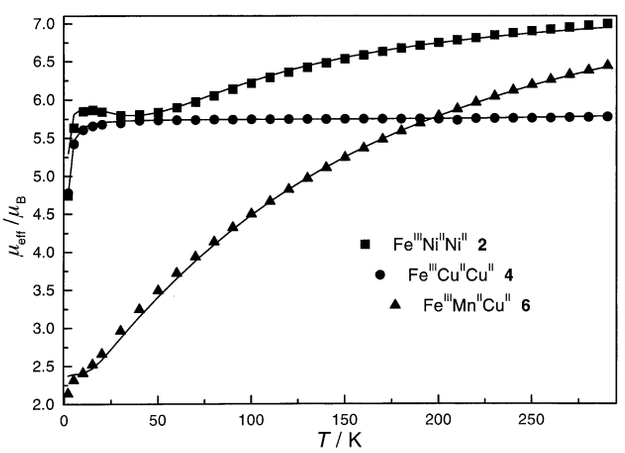

Fig. 3 Effective magnetic moment as a function of temperature for complexes **2**, **4** and **6**. The solid lines represent the simulation with the spin Hamiltonian (see text).

comparable structures.[5h,15] Thus the structure of **2** establishes that the metal centres, Fe and Ni, are in high-spin electronic configuration.

Mössbauer spectroscopy

The +3 oxidation state and the high-spin configuration of the iron centres in complexes **1**, **2**, **4**, **5** and **6** were confirmed by Mössbauer spectroscopy. The spectra were measured at 80 K and zero field, and the data are given in Table 2. They consist of asymmetrical quadrupole doublets with isomer shifts (δ) varying within the range 0.44 to 0.47 mm s^{-1} and quadrupole splitting (ΔE_Q) from 0.27 to 0.85 mm s^{-1}. The compounds Fe^{III}-$Ni^{II}Ni^{II}$ **2** and $Fe^{III}Mn^{II}Cu^{II}$ **6** exhibit values of $\Delta E_Q = 0.59$ and 0.27 mm s^{-1}, respectively. The relatively smaller values reflect significant changes in the electronic symmetry of the iron co-ordination sphere.

Magnetic susceptibility studies

Magnetic susceptibility data for polycrystalline samples were collected in the temperature range 2–295 K in order to characterise the sign and magnitude of the exchange interaction in the heterotrinuclear systems. The results are shown in Fig. 3, and Table 2.

The analysis of the magnetic data was performed using the Heisenberg–Dirac–van Vleck (HDvV) model, and the exchange interactions involved are shown pictorially below.

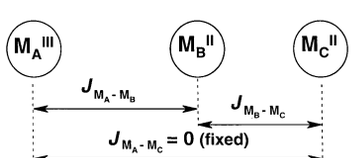

The least-squares fitting computer program JULIUS-F[16] with a full matrix diagonalisation approach was employed to fit the temperature- and field-dependent magnetisation. The program uses the spin Hamiltonian operator, $H_{total} = H_Z + H_{ZFS} + H_{HDvV}$ where the exchange coupling is described by $H_{HDvV} = -2J_{MA\text{-}MB}(S_A \cdot S_B) - 2J_{MB\text{-}MC}(S_B \cdot S_C)$. The Zeeman interaction is given by $H_Z = \mu_B B g_i S_i$ and the axial single-ion zero-field interaction by $H_{ZFS} = DS_{Zi}^2$. The axial single-ion zero-field interaction term was considered only when necessary for simulation. The spin ladders for the respective compounds were calculated without zero-field and Zeeman splitting by use of the program ENERGY.[16] The spin states $|S,S^*\rangle$ are labelled by the total spin S and subspin $S^* = S_B + S_C$ according to the Kambe notation. The results give a description of the electronic energies of the spin states of a given compound generated as a function of the J and g values obtained from the matrix diagonalisation (Table 2).

The magnetic behaviours of complexes $Fe^{III}Cu^{II}Ni^{II}$ **1** and $Co^{III}Cu^{II}Ni^{II}$ **3** have been described in previous papers[6] and are summarised here for comparison. Compound **1** exhibits an irregular spin structure with a ground state $S_T = 6/2$ arising from the antiferromagnetic nature of the couplings (see Fig. 8, later). The ground state has been confirmed by fitting the field and temperature dependent magnetisation with the parameters $g = 2.075$, $S_T = 6/2$.

Compound **3** contains a low-spin cobalt(III) ion and therefore is magnetically a binuclear system. The Cu^{II} and Ni^{II} in **3** are antiferromagnetically coupled with the first excited state, a quartet, lying 375 cm^{-1} above the doublet ground state ($S_T = 1/2$). The magnetic behaviour of $Fe^{III}Ni^{II}Ni^{II}$ **2** is depicted in Fig. 3. At 290 K the compound exhibits a μ_{eff} value of 6.99 μ_B, which is lower than the theoretical spin-only value of $\mu_{eff} = 7.14$ μ_B expected for three non-coupled spins of $S_{Fe} = 5/2$ and $S_{Ni} = S_{Ni'} = 2/2$. When the temperature is lowered μ_{eff} decreases monotonically from 6.99 μ_B at 290 K to 5.79 μ_B at 30 K. Over the range 30–10 K the curve stabilises to a plateau with $\mu_{eff} = 5.84$ μ_B. This value is very similar to that of an $S_T = 5/2$ ground state and suggests that both nickel(II) centres in the oxime ligand are strongly antiferromagnetically coupled. Below 10 K μ_{eff} decreases drastically reaching the value of 4.74 μ_B at 2 K. This behaviour is presumably due to saturation effects. The best fit yields $J_{Fe\text{-}Ni} = -9.3$ cm^{-1}, $J_{Ni\text{-}Ni'} = -21.4$ cm^{-1}, $g_{Fe} = 2.0$, $g_{Ni} = 2.28$, $D = 0$ (fixed) and confirms the antiferromagnetic nature of the couplings.

Temperature and field dependent (1,4 and 7 T) magnetisation measurements in the temperature range 2–290 K, shown in Fig. 4, further verify the ground state $S_T = 5/2$. The solid lines are simulations of the magnetisations for $S = 5/2$ with $g = 1.99$ and $D = 1.44$ cm^{-1}.

The ground state of $S_T = 5/2$ obtained from the susceptibility data is in accord with the EPR spectrum of complex **2** with effective g values of $g_x = g_y = 4.42$ and $g_z = 2.00$. The magnetic interactions operating in this linear trinuclear structure yield an $S_T = 5/2$ ground state due qualitatively to the operation of an antiferromagnetic coupling between the neighbouring nickel(II) ions. In a complex where $M_A = Fe^{III}$, $M_B = M_C = Ni^{II}$, the expected energy ladder would be composed of 1 × 1/2, 2 × 3/2, 3 × 5/2, 2 × 7/2 and 1 × 9/2 micro-states. The energy levels of the spin states using $J_{Fe\text{-}Ni}$ are shown in Fig. 5. The energy of the sextet ground term $|5/2; 0\rangle$ has been set at 0 cm^{-1}.

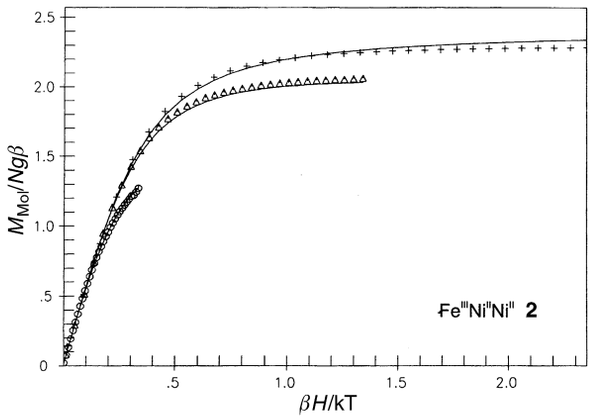

Fig. 4 Variable temperature and variable field magnetisation measurements for complex **2**. The solid lines are the simulations.

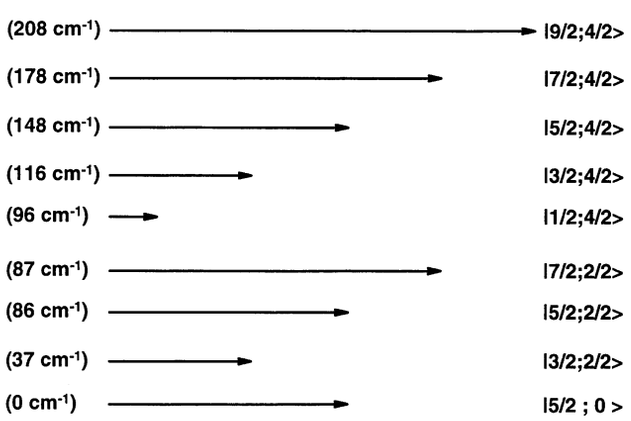

Fig. 5 Spin ladder for complex **2**.

The ground term lies 37 cm^{-1} below the first excited state, the quartet $|3/2; 2/2\rangle$.

The magnetic moment of $\mathbf{Fe^{III}Cu^{II}Cu^{II}}$ **4** remains nearly constant with μ_{eff} values varying from 5.77 to 5.73 μ_B in the temperature range 290 to 40 K. At 290 K the μ_{eff} value of 5.77 μ_B indicates the prevailing antiferromagnetic (AF) coupling, when compared with the expected value of 6.30 μ_B for an uncoupled system with $S_{Fe} = 5/2$ and $S_{Cu} = S_{Cu'} = 1/2$. From 290 to 40 K a plateau with $\mu_{eff} = 5.74\ \mu_B$ is formed. Below 40 K there is a decrease in μ_{eff} until it reaches a value of 4.77 μ_B attributable to intermolecular spin coupling. The observed effective moment of *ca.* 5.74 μ_B is very close to the expected spin only value of $\mu_{eff} = 5.92\ \mu_B$ for an $S = 5/2$ ground state of an AF coupled $Fe^{III}Cu^{II}Cu^{II}$ complex. In order to simulate the magnetic data over the whole temperature range it was necessary to consider a weak intermolecular spin coupling by introducing the Weiss constant θ. The best fit parameters $J_{Fe\text{-}Cu} = -5.0$ cm^{-1}, $J_{Cu\text{-}Cu'} = -395$ cm^{-1}, $g_{Fe} = 1.98$, $g_{Cu} = 2.10$, $\theta = -0.27$ K, $D = 0$ (fixed) confirm the antiferromagnetic nature and the magnitude of the couplings. The ground state of $S_T = 5/2$ obtained from the susceptibility data has been confirmed by fitting the experimental variable temperature magnetisation curves at 1, 4 and 7 T for $S = 5/2$ with $g = 1.94$ and $D = 0.65$ cm^{-1} and $\theta = -0.24$ K in the temperature range of 2 to 290 K (Fig. 6).

For complex **4** the following states would result: $|5/2; 0\rangle$, $|3/2; 2/2\rangle$, $|5/2; 2/2\rangle$, $|7/2; 2/2\rangle$. The first excited state, a spin quartet, lies at a considerably higher energy *ca.* 700 cm^{-1} above the isolated sextet ground state. Further confirmation of this ground state is obtained by the EPR spectrum of **4** in CH_3CN at 10 K. The spectrum was simulated for a rhombic $S = 5/2$ system with effective $g_x = 3.61$, $g_y = 4.44$ and $g_z = 4.14$, shown in Fig. 7.

The magnetic behaviour of $\mathbf{Fe^{III}Mn^{II}Cu^{II}}$ **6** is presented in Fig. 3. At 290 K the value of $\mu_{eff} = 6.44\ \mu_B$ is considerably lower

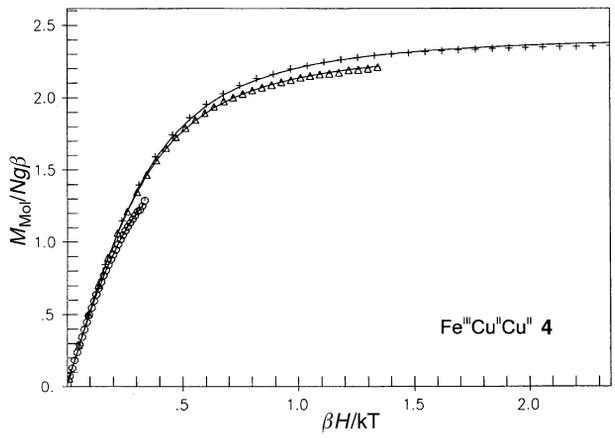

Fig. 6 Magnetisation measurements (variable field and variable temperature) for complex **4**. The simulations are shown as the solid lines (see parameters in the text).

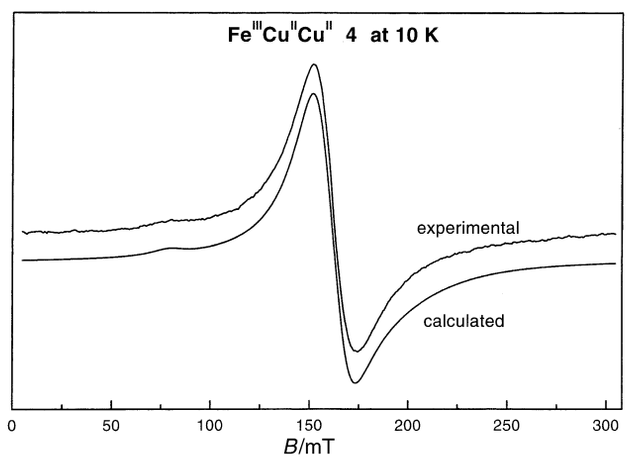

Fig. 7 X-Band EPR spectrum of complex **4** in CH_3CN at 10 K (microwave frequency 9.650 GHz, power 98.6 μW; modulation amplitude 11.43 G) together with the simulated spectrum.

than the 8.55 μ_B expected for an uncoupled system with $S_{Fe} = 5/2$, $S_{Mn} = 5/2$ and $S_{Cu} = 1/2$ indicating the presence of antiparallel spin orientation in **6**. On lowering the temperature, μ_{eff} decreases continuously and reaches a value of 2.13 μ_B at 2 K. This is not far from the spin only value of $\mu_{eff} = 1.73\ \mu_B$ for $S = 1/2$ expected as the ground state for an antiferromagnetically coupled $Fe^{III}Mn^{II}Cu^{II}$ complex. The best fit results in $J_{Fe\text{-}Mn} = -12.6$ cm^{-1}, $J_{Mn\text{-}Cu} = -66.8$ cm^{-1}, $g_{Fe} = 2.00$, $g_{Mn} = 2.00$ and $g_{Cu} = 2.10$. For this compound the following sequential order of the spins results: $|1/2; 4/2\rangle$ at 0 cm^{-1} (arbitrarily chosen), $|3/2; 4/2\rangle$ at 43 cm^{-1}, $|5/2; 4/2\rangle$ at 115 cm^{-1}, $|7/2; 4/2\rangle$ at 216 cm^{-1}, and the other excited states are $|9/2; 4/2\rangle$, $|1/2; 6/2\rangle$, $|3/2; 6/2\rangle$, $|5/2; 6/2\rangle$, $|7/2; 6/2\rangle$, $|9/2; 6/2\rangle$ and $|11/2; 6/2\rangle$, all above 220 cm^{-1}. Thus the ground term lies 43 cm^{-1} below the first excited quartet $|3/2; 4/2\rangle$ state.

Finally, we examined the compound $\mathbf{Fe^{III}Ni^{II}Cu^{II}}$ **5** which is isoelectronic to $\mathbf{Fe^{III}Cu^{II}Ni^{II}}$ **1**. As will be shown the topological features influence strongly the magnetochemical properties of the compounds. On lowering the temperature, μ_{eff} decreases monotonically from 6.14 μ_B at 290 K until a plateau is reached in the temperature range 20–10 K with μ_{eff} varying from 4.73 to 4.69 μ_B. These values are very close to the spin only value of $\mu_{eff} = 4.89\ \mu_B$ for an $S = 4/2$ spin state, expected as the ground state of an antiferromagnetically coupled $\mathbf{Fe^{III}Ni^{II}Cu^{II}}$ complex. Below 10 K μ_{eff} further decreases due to saturation effects. The best fit results in $J_{Fe\text{-}Ni} = -10.64$ cm^{-1}, $J_{Ni\text{-}Cu} = -161.5$ cm^{-1}, $g_{Fe} = 2.00$, $g_{Ni} = 2.30$ and $g_{Cu} = 2.10$. In contrast to the compound $\mathbf{Fe^{III}Cu^{II}Ni^{II}}$ **1** where the magnetic interactions result in a ground state of high-spin multiplicity ($S_T = 6/2$), this linear

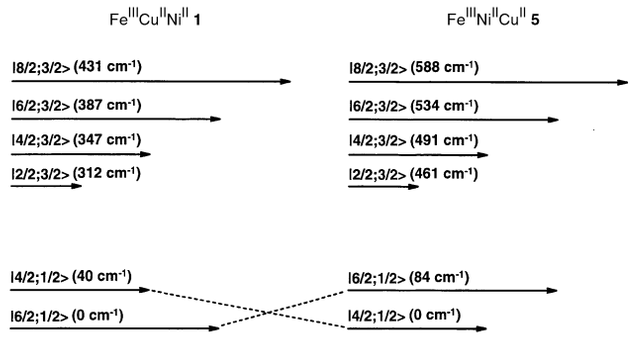

Fig. 8 Low-lying energy levels for **Fe^{III}Ni^{II}Cu^{II} 5** and **Fe^{III}Cu^{II}Ni^{II} 1**.

trinuclear structure **5** yields an $S_T = 4/2$ ground state resulting also from an antiparallel spin alignment. As a direct consequence, the energy ladder for **5** is very similar to that of the isoelectronic **1**, but with *inverted* ground and first excited states as shown in Fig. 8. The values are not to scale and the ground state energy has been set at 0 cm^{-1}. The lengths of the arrows correspond to the degeneracies of the levels. For **5** the ground state is the quintet $|4/2; 1/2\rangle$ that lies 84 cm^{-1} below the first excited septet state $|6/2; 1/2\rangle$, whereas for **1** the excited quintet lies 40 cm^{-1} above the septet ground term.

Rationale for the mechanism of the exchange interactions. In this section a qualitative rationalisation for the exchange mechanisms between nearest neighbouring and terminal spin carriers in the heterotrinuclear complexes is attempted. Although the general approach will be extended to all the $M_AM_BM_C$ members, this rationale starts with the complexes which have been structurally characterised, namely **Fe^{III}Cu^{II}Ni^{II} 1**, **Fe^{III}Ni^{II}Ni^{II} 2** and **Co$^{III}_{l.s.}$Cu^{II}Ni^{II} 3**.

The $M_A \cdots M_B$ separation is *ca.* 3.75 Å and the $M_B \cdots M_C$ separation *ca.* 3.1 Å. These distances are large enough to ensure that no direct interaction between the spin carriers occurs. Therefore the observed spin couplings arise *via* a superexchange pathway along the frame $\mathbf{M_A}$–O–N–$\mathbf{M_B}$–O–$\mathbf{M_C}$ with the oxygen and nitrogen atoms of the bridging oxime groups and of the phenolates sp^2 hybridised. The magnetic orbitals for the different metal ions are given by simple ligand-field considerations. Following the Goodenough–Kanamori rules[17] the extent of overlap between the metal magnetic orbitals is responsible for the appearance of antiferromagnetic interactions, whereas orthogonality (or symmetry-forbidden overlap) of the same orbitals induces ferromagnetic contributions. With these ideas in mind, it is possible to correlate the spin–spin coupling to the crystal structures of the complexes. The evaluated overall exchange coupling constant J thus results from individual antiferromagnetic and ferromagnetic exchange interactions: $J = J_{AF} + J_F$. The term J_{AF} constitutes a negative contribution and favours antiparallel electron pairing, whereas the term J_F constitutes a positive contribution. Finally, due to the possibility of fixing the remote coupling constant J_{AC} between the first and the third metal centres (>6.5 Å) as zero in all compounds,[18] it is assumed that the exchange interactions are essentially σ in nature. Nevertheless, this postulate only implies the *predominance* of these σ interactions over the insignificant π interactions.

In the compound **Fe^{III}Cu^{II}Ni^{II} 1** the local symmetry on the iron(III) ion assumes C_{2v} geometry by considering the similarity of Fe–Cl and Fe–N bonds. The environment around the Fe^{III} is trigonal with a $t_{2g^3}e_{g^2}$ high spin configuration. The Cu^{II}-ion shows a local C_S symmetry with the unpaired electron in the $(d_{x^2-y^2})^1$ orbital. The Ni^{II} with a $t_{2g}{}^6e_g{}^2$ configuration and magnetic orbitals $(d_{x^2-y^2})^1$ and $(d_{z^2})^1$ also assumes a C_{2v} symmetry in a tetragonally elongated distorted octahedron. The $d_{x^2-y^2}$ magnetic orbitals of the three transition metal ions point toward their four nearest neighbours and interact with each other through the oximato (Fe–Cu) and phenolato (Cu–Ni) bridges. This interaction can be described using the Ginsberg[19] notation as being Fe($d_{x^2-y^2}$) ‖sp^2‖ Cu($d_{x^2-y^2}$) ‖sp$^2_{(O)}$‖ Ni($d_{x^2-y^2}$), where the term ‖sp^2‖ abbreviates the σ superexchange mechanism ‖sp$^2_{(O)}$‖sp$^2_{(N)}$‖ in the oximato bridge. This antiferromagnetic coupling although dominant is reduced by ferromagnetic couplings also present in the system. The principal ferromagnetic contributions are described as Fe(t_{2g} parentage) ‖sp$^2_{(O)}$ ⊥ sp$^2_{(N)}$‖ Cu(d_{z^2}) and Cu($d_{x^2-y^2}$) ‖sp$^2_{(O)}$ ⊥ Ni (d_{xy}).

In case of the structurally characterised **Co^{III}Cu^{II}Ni^{II} 3** the same arguments are valid since no spin interaction is possible between the low spin Co^{III} and its neighbours. With the formation of a μ-OH bridge between the Co^{III} and the Cu^{II}, the latter centre assumes a more distorted geometry in comparison to that in compound **1** with subsequent loss of linearity of the Co–Cu–Ni skeleton, which may be responsible for the small increase in the strength of exchange coupling of $J_{Cu\text{-}Ni}$ from −118.6 in **1** to −130.2 cm^{-1} in **3**.

Finally, comparison of the compound **Fe^{III}Ni^{II}Ni^{II} 2** with **1** shows that the $-J$ values decrease drastically: $-J_{AB}$ falls from 19.8 to 9.3 cm^{-1} and $-J_{BC}$ from 118.6 to 21.4 cm^{-1}. Such reduction is however expected and explained by the fact that there is one more unpaired electron in Ni^{II} compared with the d^9 system. An extra pathway, ferromagnetic in nature, involves the d_{z^2} and $d_{x^2-y^2}$ orbitals of each vicinal nickel ion and is described as Ni(d_{z^2}) ‖ sp^2 ⊥ Ni′($d_{x^2-y^2}$). Although the antiferromagnetic pathway ($d_{x^2-y^2}$) ‖ ($d_{x^2-y^2}$) still dominates the overall exchange, this ferromagnetic contribution results in reduction of the net antiferromagnetic coupling between the spin carriers. Although both nickel ions possess a $(d_{z^2})^1$ orbital, no significant contribution is expected due to insignificant overlap.

Analysing the compound **Fe^{III}Cu^{II}Cu^{II} 4**, the presence of a single electron in each d^9 centre in close proximity presupposes a strong antiferromagnetic coupling along the ($d_{x^2-y^2}$) ‖sp$^2_{(O)}$‖ ($d_{x'^2-y'^2}$) pathway. The $J_{Cu\text{-}Cu}$ of −395 cm^{-1} is in good agreement with the values reported for similar systems.[20] The weak $J_{Fe\text{-}Cu(1)}$ coupling constant (*cf.* ref. 3*f*) in comparison to the similar interactions between Fe^{III} and Cu^{II} is noteworthy.

Fe^{III}Ni^{II}Cu^{II} 5 is the electronic analogue of complex **1**. In conjunction with the magnetic pathways described above, additional ferromagnetic contributions reduce the magnitude of the Fe–Ni coupling. These new contributions are described as Fe(d_{xz},d_{yz}) ‖ sp^2 ⊥ Ni(d_{z^2}). Owing to the interactions with the Fe^{III}, the ferromagnetic contribution to the coupling between nickel and copper is diminished leading to an increase in the strength of the net antiferromagnetic coupling from −118.6 cm^{-1} for **1** to −161.5 cm^{-1} for **5**.

Finally, in compound **Fe^{III}Mn^{II}Cu^{II} 6** the antiferromagnetic pathway still dominates the overall interaction. This pathway can be summarised as Fe($d_{x^2-y^2}$) ‖ Mn($d_{x^2-y^2}$) ‖ Cu($d_{x^2-y^2}$). The Fe–Mn interaction involves several parallel couplings so that the order of magnitude of −12 cm^{-1} is in agreement with the expected value[21] for a d^5–d^5 system. It was observed that the substitution of a given metal M_B in binuclear complexes with Cu–M_B frameworks, where M_B is in an octahedral or pseudo-octahedral environment, dictates a factor $J_{Cu\text{-}M1}/J_{Cu\text{-}M2} > 2.0$ due to the energy difference δ between the magnetic orbitals of the two metal sites M^1 and M^2.[5b,22] Considering the substitution of Ni^{II} by Mn^{II} the magnitude of the antiferromagnetic coupling is expected to decrease by a factor of 2.5. J_{BC} values for the compounds **Fe^{III}Ni^{II}Cu^{II}** and **Fe^{III}Mn^{II}Cu^{II}** differ by a factor of |−161.5/−66.8| = 2.4. The results described here confirm the predominance of σ-exchange pathways, which vary from moderate to strong interactions. The Goodenough–Kanamori rules are able to explain the nature of the interactions and the strength of the overall antiferromagnetic interactions decreases in the following order: FeCuCu > FeNiCu > FeCuNi > FeMnCu > FeNiNi. Owing to the symmetry properties of the σ interactions the dominant antiferromagnetic

pathway involves the $d_{x^2-y^2}$ orbitals in each of the complexes studied. Considering the whole $M_AM_BM_C$ network the molecules assume a C_S symmetry in which the original orbitals transform to the following: $d_{x^2-y^2}$, d_{z^2}, $d_{xy} \longrightarrow A'$ and d_{xz}, $d_{yz} \longrightarrow A''$. The principal antiferromagnetic interaction is thus better described as $A'_{MA}\|sp^2\|A'_{MB}\|sp^2{}_{(O)}\|A'_{MC}$. This does not operate alone but competes with several other ferromagnetic pathways. Despite this competition, the antiferromagnetic interactions dominate the ferromagnetic ones and have greater influence over the overall magnetic pathway.

Concluding remarks

The modular complexes **1**, **3**, **4** and **6** presented are the *first examples* of exchange coupled asymmetric linear complexes containing three different metals and were synthesized by use of selective template reactions involving the imine–oxime ligand H_4Lox. This ligand supports the binding of similar or dissimilar metals and reacts with a third metal, co-ordinated facially to a tmtacn unit acting as an end-cap ligand and preventing further undesirable reactions. The limitation of the synthetic method is the *scrambling* effect among the metal centres; designing of new oxime ligands is required to accomplish cores with ions such as Cr^{III}, Mn^{II}, Mn^{III}, Fe^{II}, Fe^{III} and Zn^{II}. The use of ligands with incorporated pendant arms might increase selectivity favouring the stabilisation of different species as well as different exchange coupling and will be the subject of future research work.

Experimental

Chemicals

Solvents and reagents were obtained from commercial sources and used without further purification. 1,4,7-Trimethyl-1,4,7-triazacyclononane[23] and the precursor aldehyde Hdfmp[6] (Hdfmp = 2,6-diformyl-4-methylphenol) were prepared according to previous published methods. The mononuclear precursors $[M_C^{II}L]$ (M_C = Ni or Cu) as well as the binuclear precursors $[M_C^{II}M_B^{II}L]Cl_2$ (M_B = Cu^{II}, Ni^{II} or Mn^{II}) were obtained by modifications of the published procedure.[9]

Physical measurements

IR spectra were measured from 4000 to 400 cm^{-1} as KBr pellets at room temperature on a Perkin-Elmer FT-IR-Spectrophotometer 2000. Elemental analyses were performed by the "Mikroanalytisches Labor H. Kolbe", in Mülheim. UV-vis spectra of 5.0×10^{-4} M solutions in CH_3CN were recorded on a Perkin-Elmer UV/Vis Spectrophotometer Lambda 19 in the range 200 to 1200 nm. The magnetochemical measurements of the powdered samples were performed in a Quantum Design SQUID-Magnetometer MPMS generally in a field of 1 T. The samples were put in gelatine capsules and the response function was measured four times for each 32 measured temperature points. Diamagnetic contributions were estimated for each compound by making use of Pascal's constants. Mössbauer data were recorded on alternating constant-acceleration spectrometers. The minimum experimental linewidth was 0.24 mm s^{-1} full width at half maximum. The sample temperature was kept constant at 80 K either in an Oxford Variox or an Oxford Mössbauer-Spectromag cryostat. ^{57}Co/Rh was used as the radiation source. The measurements were carried out with solid samples containing the isotope ^{57}Fe and the isomer shifts are given relative to α-Fe at room temperature. The X-band EPR spectra of the polycrystalline materials either as solids or in solution were recorded at various temperatures between 10 and 100 K with a Bruker ESP 300 spectrometer equipped with a standard TE 102 cavity, an Oxford Instruments liquid helium continuous-flow cryostat, an NMR gaussmeter, and a frequency meter.

Table 3 Crystal data and structure refinement for $Fe^{III}Ni^{II}Ni^{II}$ **2**

Empirical formula	$C_{37}H_{51}FeN_{12}Ni_2O_6S_3$
Formula weight	1029.35
T/K	293(2)
Crystal system	Monoclinic
Space group	$P2_1/c$
a/Å	14.095(2)
b/Å	15.534(3)
c/Å	21.134(4)
β/°	98.38(2)
V/Å^3	4577.9(14)
Z	4
μ/mm^{-1}	1.321
Reflections collected	19035
Independent reflections	7010 (R_{int} = 0.1004)
Final $R1$, $wR2$ [$I > 2\sigma(I)$]	0.0529, 0.1119
(all data)	0.1203, 0.1294

Crystallography

X-Ray diffraction data of a dark red crystal of $Fe^{III}Ni^{II}Ni^{II}$ **2** were collected on a Nonius Kappa CCD diffractometer. Crystal data are summarised in Table 3. Graphite-monochromatised Mo-Kα radiation with $\lambda = 0.71073$ Å was employed and unit cell parameters were determined from a least-squares fit of 6370 reflections. Data were corrected for Lorentz and polarisation effects. The structure was solved by direct methods and subsequent Fourier-difference techniques, and refined anisotropically by full-matrix least squares on F^2 with the program SHELXTL PLUS.[24] Hydrogen atoms were geometrically attached and included in the refinement.

CCDC reference number 186/2212.

See http://www.rsc.org/suppdata/dt/b0/b005768l/ for crystallographic files in .cif format.

Syntheses

The synthons $[M_C^{II}M_B^{II}(Lox)]Cl$. Owing to the similarities among the syntheses a general description is given. The binuclear precursor $[M_C^{II}M_B^{II}(L)]Cl_2$ (1 mmol) was suspended in 30 cm^3 of MeOH. Simultaneously $NH_2OH{\cdot}HCl$ (3 mmol) was dissolved in 10 cm^3 of MeOH and neutralised with Et_3N (4 mmol). Both solutions were mixed under vigorous stirring and heated to 60 °C in a water-bath for *ca.* 1 h. A greenish or brownish powder precipitated, was filtered off under vacuum and then washed with 2-propanol and diethyl ether. $[Ni^{II}Cu^{II}$-(Lox)]Cl·$2H_2O$: $C_{21}H_{26}N_4O_6ClCuNi$ (% calc./found) C 42.96/43.1; H 4.29/4.4; Cu 10.83/10.9; N 9.54/9.3; Ni 10.00/9.7; IR (KBr, cm^{-1}) 1634 ν(CN); 1314 δ(Ph–O); 1235, 1189 ν(NO); yield 0.43 g (73%). $[Ni^{II}_2(Lox)]Cl{\cdot}2H_2O$: $C_{23}H_{33}ClN_4Ni_2O_8$ (% calc./found) C 42.74/42.5; H 5.15/4.9; N 8.67/9.0; Ni 18.16/18.2; IR (KBr, cm^{-1}) 1633 ν(CN); 1321 δ(Ph–O); 1232, 1187 ν(NO); yield 0.43 g (68%). $[Cu^{II}_2(Lox)]Cl{\cdot}2H_2O$: $C_{21}H_{25}ClCuN_4O_6$ (% calc./found) C 42.61/42.3; H 4.26/4.1; Cu 21.47/21.6; N 9.46/9.6; IR (KBr, cm^{-1}) 1632 ν(CN); 1310 δ(Ph–O); 1238, 1194 ν(NO); yield 0.43 g (72%). $[Cu^{II}Ni^{II}(Lox)]Cl{\cdot}2H_2O$: $C_{21}H_{26}$-$ClCuN_4NiO_6$ (% calc./found) C 42.96/43.2; H 4.29/4.4; Cu 10.82/10.8; N 9.54/9.6; Ni 10.00/10.2; IR (KBr, cm^{-1}) 1633 ν(CN); 1316 δ(Ph–O); 1235 ν(NO); yield 0.41 g (70%). $[Cu^{II}$-Mn^{II}(Lox)]Cl·H_2O: $C_{21}H_{23}ClCuMnN_4O_5$ (% calc./found) C 44.61/44.9; H 4.10/4.2; Cu 11.24/11.3; Mn 9.72/9.9; N 9.91/9.8; IR (KBr, cm^{-1}) 1624 ν(CN); 1306 δ(Ph–O); 1236, 1194 ν(NO); yield 0.41 g (70%).

$[(tmtacn)Fe^{III}(Cl)Cu^{II}(MeOH)Ni^{II}(MeOH)_2(Lox)][ClO_4]_2{\cdot}H_2O$ 1. A solid sample of $[Fe^{III}LCl_3]$ (0.17 g, 0.5 mmol) was added in small portions to a suspension of $[Ni^{II}Cu^{II}$-(HLox)]Cl·$2H_2O$ (0.29 g, 0.5 mmol) in 50 cm^3 of MeOH. Addition of 0.5 cm^3 Et_3N to the suspension led to a dark brown solution that was stirred at 80 °C in a water-bath for 1 hour and afterwards filtered while still warm to remove any solid or unchanged material. Solid $NaClO_4{\cdot}H_2O$ (≈0.5 g) was added

carefully with stirring. Upon standing at ambient temperature the solution deposited brown crystals which were filtered off and collected. $C_{33}H_{55}Cl_3CuFeN_7NiO_{16}$ (% calc./found) C 36.46/37.52; H 5.10/5.20; Cu 5.83/5.56; Fe 5.15/5.25; N 9.02/9.40; Ni 5.38/5.53; IR (KBr pellets, cm^{-1}) 2924, 2868 $\nu(CH_3)$; 1636 ν(CN); 1086 (ClO_4); UV-vis in MeCN solution [λ_{max}/nm (ε/M^{-1} cm^{-1})] 365 (3780), 450sh (≈1150) and 567sh (≈551); yield 0.42 g (78%).

[(tmtacn)Fe^{III}(NCS)Ni^{II}(H_2O)(NCS)Ni^{II}(NCS)(H_2O)(Lox)]·2MeCN 2. A solid sample of [$Fe^{III}LCl_3$] (0.17 g, 0.5 mmol) was added to a suspension of [Ni^{II}_2(HLox)]Cl·$2H_2O$ (0.33 g, 0.5 mmol) in 50 cm^3 of MeOH. Addition of 0.5 cm^3 Et_3N to the suspension led to a brown solution that was stirred at 80 °C in a water-bath for 1 hour and afterwards filtered while warm. Solid NaSCN (≈0.5 g) was added and the solution briefly heated. Recrystallisation in MeCN gave dark crystals. $C_{37}H_{51}FeN_{12}Ni_2O_6S_3$ (% calc./found) C 43.18/42.83; H 4.99/4.94; Fe 5.43/5.45; N 16.33/15.82; Ni 11.40/11.73; IR (KBr pellets, cm^{-1}) 2975, 2915 $\nu(CH_3)$; 1632 ν(CN); 1189, 1234 ν(NO); 2100, 1055 (SCN); UV-vis in MeCN solution [λ_{max}/nm (ε/M^{-1} cm^{-1})] 378 (3420), 453sh (≈1070) and 560 (674); yield 0.37 g (69%).

[(tmtacn)Co^{III}(μ-OH)$Cu^{II}Ni^{II}$(H_2O)$_2$(Lox)][ClO_4]$_2$·MeOH·2H_2O 3. The synthesis of this compound was described elsewhere.[6]

[(tmtacn)Fe^{III}(Cl)Cu^{II}(H_2O)Cu^{II}(H_2O)(Lox)][ClO_4]$_2$ 4. A solid sample of [$Fe^{III}LCl_3$] (0.17 g, 0.5 mmol) was added in small portions to a suspension of [Cu^{II}_2(HLox)]Cl·$2H_2O$ (0.30 g, 0.5 mmol) in 50 cm^3 of MeOH. Addition of 0.5 cm^3 Et_3N to the suspension led to a dark brown solution that was stirred in a water-bath at 80 °C for 1 hour and afterwards filtered while still warm. $NaClO_4$·H_2O (0.5 g) was added. After some time the solution deposited a brown powder which was filtered off and air-dried. $C_{30}H_{44}Cl_3Cu_2FeN_7O_{14}$ (% calc./found) C 35.47/35.45; H 4.37/4.58; Cu 12.51/12.52; Fe 5.50/5.42; N 9.65/9.60; IR (KBr pellets, cm^{-1}) 2927, 2871 $\nu(CH_3)$; 1628 ν(CN); 1091 (ClO_4); UV-vis in MeCN solution [λ_{max}/nm (ε/M^{-1} cm^{-1})] 360 (2990) and 546sh (≈231); yield 0.38 g (72%).

[(tmtacn)Fe^{III}(Cl)Ni^{II}(H_2O)$_2$$Cu^{II}$($H_2O$)(Lox)][$ClO_4$]$_2$ 5. A solid sample of [$Fe^{III}LCl_3$] (0.17 g, 0.5 mmol) was added to a suspension of [$Cu^{II}Ni^{II}$(HLox)]Cl·$2H_2O$ (0.29 g, 0.5 mmol) in 50 cm^3 of MeOH. Addition of 0.5 cm^3 Et_3N to the suspension led to a dark brown solution that was stirred in a water-bath at 80 °C for 1 hour and then filtered while warm. Solid $NaClO_4$·H_2O (0.5 g) was added and after 48 hours at ambient temperature the solution deposited brown micro-crystals which were filtered off and collected. $C_{30}H_{47}Cl_3CuFeN_7NiO_{15}$ C 35.05/35.94; H 4.61/4.62; Cu 6.13/6.30; Fe 5.45/5.48; N 9.57/9.71; IR (KBr pellets, cm^{-1}) 2924, 2882 $\nu(CH_3)$; 1631 ν(CN); 1092 (ClO_4); UV-vis in MeCN solution [λ_{max}/nm (ε/M^{-1} cm^{-1})] 375 (3200), 461sh (≈1040) and 548sh (≈634); yield 0.42 g (82%).

[(tmtacn)Fe^{III}(Cl)Mn^{II}(MeOH)$_2$$Cu^{II}$($H_2O$)(Lox)][$ClO_4$]$_2$ 6. A solid sample of [$Fe^{III}LCl_3$] (0.17 g, 0.5 mmol) was added in small portions to a suspension of [$Cu^{II}Mn^{II}$(HLox)]Cl·H_2O (0.28 g, 0.5 mmol) in 50 cm^3 of MeOH. Addition of 0.5 cm^3 Et_3N led to a dark brown solution which was stirred in a water-bath at 80 °C for 1 hour and filtered while still warm. Solid $NaClO_4$·H_2O (0.5 g) was added with stirring. After 24 h upon standing at ambient temperature the solution deposited a brown powder which was filtered off and air-dried. $C_{32}H_{51}CuFeMnN_7O_{15}$ (% calc./found) C 36.45/35.10; H 4.87/4.54; Fe 5.30/5.19; Mn 5.21/5.20; Cu 6.03/6.10; N 9.30/9.15; IR (KBr pellets, cm^{-1}) 2922, 2867 $\nu(CH_3)$; 1627 ν(CN); 1087 (ClO_4); UV-vis in MeCN solution [λ_{max}/nm (ε/M^{-1} cm^{-1})] 382 (2960) and 532sh (≈483); yield 0.35 g (68%).

CAUTION: Although no difficulties were experienced with handling of the compounds isolated as their perchlorate salts, extreme caution is needed due to the unpredictable behaviour of such compounds.

Acknowledgements

The authors thank the Fonds der Chemischen Industrie and the Max-Planck-Society for financial support. C. N. V. thanks the Deutsche Akademischer Austauschdienst (DAAD) for a fellowship. Technical assistance of Mrs H. Schucht and Mr A. Göbbels is gratefully acknowledged.

References

1 K. S. Murray, *Adv. Inorg. Chem.*, 1995, **43**, 261; O. Kahn, *Adv. Inorg. Chem.*, 1995, **43**, 179; O. Kahn, *Molecular Magnetism*, VCH Verlagsgesellschaft, Weinheim, 1993; *Research Frontiers in Magnetochemistry*, ed. C. J. O'Connor, World Scientific, Singapore, 1993; *Magnetic Molecular Materials*, eds. D. Gatteschi, O. Kahn, J. S. Miller and F. Palacio, Kluwer Academic Publishers, Dordrecht, 1991.

2 R. H. Holm and E. I. Solomon, *Chem. Rev.*, 1996, **96**, 7; S. J. Lippard and J. M. Berg, *Principles of Bioinorganic Chemistry*, University Science Books, Mill Valley, CF, 1994; *Bioinorganic Chemistry of Copper*, eds. K. D. Karlin and Z. Tyeklár, Chapman & Hall, New York, 1993.

3 (*a*) S. J. Gruber, C. M. Harris and E. Sinn, *J. Inorg. Nucl. Chem.*, 1968, **30**, 1805; (*b*) J. Selbin and L. Ganguly, *J. Inorg. Nucl. Chem. Lett.*, 1969, **5**, 815; (*c*) C. B. Singh and B. Sahoo, *J. Inorg. Nucl. Chem.*, 1974, **36**, 1259; (*d*) R. L. Linkvedt, L. S. Kramer, G. Ranger, P. W. Corfield and M. D. Glick, *Inorg. Chem.*, 1983, **22**, 3580; (*e*) D. Luneau, H. Oshio, H. Okawa and S. Kida, *J. Chem. Soc., Dalton Trans.*, 1990, 2283; (*f*) P. Chaudhuri, M. Winter, P. Fleischhauer, W. Haase, U. Flörke and H.-J. Haupt, *J. Chem. Soc., Chem. Commun.*, 1990, 28.

4 P. Chaudhuri, M. Hess, E. Rentschler, T. Weyhermüller and U. Flörke, *New J. Chem.*, 1998, **22**, 553; (*b*) E. Bill, C. Krebs, M. Winter, M. Gerdan, A. X. Trautwein, U. Flörke, H.-J. Haupt and P. Chaudhuri, *Chem. Eur. J.*, 1997, **3**, 193.

5 (*a*) P. Chaudhuri, M. Winter, U. Flörke and H.-J. Haupt, *Inorg. Chim. Acta*, 1995, **232**, 125; (*b*) F. Birkelbach, M. Winter, U. Flörke, H.-J. Haupt, C. Butzlaff, M. Lengen, E. Bill, A. X. Trautwein, K. Wieghardt and P. Chaudhuri, *Inorg. Chem.*, 1994, **33**, 3990; (*c*) D. Burdinski, F. Birkelbach, M. Gerdan, A. X. Trautwein, K. Wieghardt and P. Chaudhuri, *J. Chem. Soc., Chem. Commun.*, 1995, 963; (*d*) P. Chaudhuri, M. Winter, B. P. C. Della Vedova, E. Bill, A. X. Trautwein, S. Gehring, P. Fleischhauer, B. Nuber and J. Weiss, *Inorg. Chem.*, 1991, **30**, 2148; (*e*) D. Burdinski, F. Birkelbach, T. Weyhermüller, U. Flörke, H.-J. Haupt, M. Lengen, A. X. Trautwein, E. Bill, K. Wieghardt and P. Chaudhuri, *Inorg. Chem.*, 1998, **37**, 1009; (*f*) F. Birkelbach, U. Flörke, H.-J. Haupt, C. Butzlaff, A. X. Trautwein, K. Wieghardt and P. Chaudhuri, *Inorg. Chem.*, 1998, **37**, 2000 and references therein; (*g*) P. Chaudhuri, F. Birkelbach, M. Winter, V. Staemmler, P. Fleischhauer, W. Haase, U. Flörke and H.-J. Haupt, *J. Chem. Soc., Dalton Trans.*, 1994, 2313; (*h*) C. Krebs, M. Winter, T. Weyhermüller, E. Bill, K. Wieghardt and P. Chaudhuri, *J. Chem. Soc., Chem. Commun.*, 1995, 1913 and references therein.

6 (*a*) C. N. Verani, T. Weyhermüller, E. Rentschler, E. Bill and P. Chaudhuri, *Chem. Commun.*, 1998, 2475; (*b*) C. N. Verani, E. Rentschler, T. Weyhermüller, E. Bill and P. Chaudhuri, *J. Chem. Soc., Dalton Trans.*, 2000, 251.

7 E. V. Rybak-Akimova, D. H. Busch, P. K. Kahol, N. Pinto, N. W. Alcock and H. J. Clase, *Inorg. Chem.*, 1997, **36**, 510.

8 H. Okawa and S. Kida, *Bull. Chem. Soc. Jpn.*, 1972, **45**, 1759; D. Black, A. J. Blake, K. P. Dancey, A. Harrison, M. McPartlin, S. Parsons, P. A. Tasker, G. Whittaker and M. Schröder, *J. Chem. Soc., Dalton Trans.*, 1998, 3953.

9 R. R. Gagné, C. L. Spiro, T. J. Smith, C. A. Hamann, W. R. Thies and A. K. Shiemke, *J. Am. Chem. Soc.*, 1981, **103**, 4073.

10 B. Egneus, *Talanta*, 1972, **19**, 1387; K. Burger, L. Ruff and F. Ruff, *J. Inorg. Nucl. Chem.*, 1965, **27**, 179; A. Chakravorty, *Coord. Chem. Rev.*, 1974, **13**, 1.

11 C. Fraser and B. Bosnich, *Inorg. Chem.*, 1994, **33**, 338; K. K. Nanda, S. Mohanta, U. Flörke, S. K. Dutta and K. Nag, *J. Chem. Soc., Dalton Trans.*, 1995, 3831; H. Golchoubian, W. L. Waltz and J. W. Quail, *Can. J. Chem.*, 1999, **77**, 37.

12 C. J. O'Connor, D. P. Freyberg and E. Sinn, *Inorg. Chem.*, 1979, **18**, 1077.
13 T. Aono, H. Wada, Y. Aratake, N. Matsumoto, H. Okawa and Y. Matsuda, *Chem. Commun.*, 1996, 25.
14 C. K. Johnson, ORTEP II, Report ORNL-5138, Oak Ridge National Laboratory, Oak Ridge, TN, 1976.
15 X. Chen, S. Zhan, C. Hu, Q. Meng and J. Shun, *Inorg. Chim. Acta*, 1997, **260**, 95; W. Yan, C. Ma, J. Wu, W. Zhang and D. Jiang, *Inorg. Chim. Acta*, 1999, **287**, 212.
16 V. Staemmler, C. Krebs and F. Birkelbach, unpublished computer program, Bochum, 1997.
17 J. B. Goodenough, *Phys. Rev.*, 1955, **100**, 564; J. Kanamori, *J. Phys. Chem. Solids*, 1959, **10**, 87; J. B. Goodenough, *Magnetism & Chemical Bond*, Wiley, New York, 1963.
18 Using compound **1** as an example, another acceptable solution involves consideration of a small coupling between M_A and M_C (<3.0 cm^{-1}). This coupling led to a small decrease of the *g* values and consequent increase of the separation in the energetic levels from 40 to 52 cm^{-1} between the ground term $|6/2;1/2\rangle$ and the first excited term $|4/2;1/2\rangle$. Since $|J_{BC}| = 118.6$ $cm^{-1} \gg |J_{AB}| = 19.8$ $cm^{-1} \gg |J_{AC}| = 3.0$ cm^{-1} the last coupling was set to zero in order to avoid overparametrisation and to simplify comparisons among the complexes.
19 A. P. Ginsberg, *Inorg. Chim. Acta Rev.*, 1971, **5**, 45.
20 L. K. Thompson, S. K. Mandal, S. S. Tandon, J. N. Bridson and M. K. Park, *Inorg. Chem.*, 1996, **35**, 3117.
21 M. Lengen, E. Bill, C. Butzlaff, A. X. Trautwein, M. Winter and P. Chaudhuri, *Hyperfine Interact.*, 1994, **94**, 1849; T. R. Holman, Z. Wang, M. P. Hendrich and L. Que, Jr., *Inorg. Chem.*, 1995, **34**, 134.
22 P. Tola, O. Kahn, C. Chauvel and H. Coudanne, *Nouv. J. Chim.*, 1979, **1**, 467.
23 K. Wieghardt, P. Chaudhuri, B. Nuber and J. Weiss, *Inorg. Chem.*, 1982, **21**, 3086; P. Chaudhuri, M. Winter, K. Wieghardt, S. Gehring, W. Haase, B. Nuber and J. Weiss, *Inorg. Chem.*, 1988, **27**, 1564.
24 G. M. Sheldrick, SHELXTL PLUS Program package (PC version), Siemens Analytical X-Ray Instruments Inc., Madison, WI, 1990.